Earth and Planetary Science Letters, 118 (1993) 145–166
Elsevier Science Publishers B.V., Amsterdam

[vdV]

Magnetostratigraphic calibration of the Late Valanginian carbon isotope event in pelagic limestones from Northern Italy and Switzerland

J.E.T. Channell, E. Erba and A. Lini

[a] *Department of Geology, University of Florida, Gainesville, FL 32611, USA*
[b] *Dipartimento di Scienze della Terra, Università di Milano, 20133 Milan, Italy*
[c] *Geologisches Institut, ETH Zentrum, 8092 Zürich, Switzerland*

Received January 7, 1993; revision accepted May 24, 1993

ABSTRACT

Magnetostratigraphic, biostratigraphic and carbon isotope data are presented from five Lower Cretaceous pelagic limestone sections in the Southern Alps. A positive carbon isotope event is recorded in bulk carbonate from the Upper Valanginian of all five sections, and the magnetostratigraphy and biostratigraphy provide the age model. The record of the isotope event in absolute time is closely replicated in all five sections. As the sections are located in two paleogeographic basins and are separated by up to 300 km, the synchronous isotope event cannot be interpreted as an artifact of diagenesis. A reduction in magnetization intensity coincident with the $\delta^{13}C$ peak may be due to diagenetic magnetite dissolution enhanced by increased organic carbon burial.

According to the age model, which uses GTS89 timescale [1], background $\delta^{13}C$ values of 1.5‰ are recorded from 145 to 137 Ma. Between 137 and 136 Ma, $\delta^{13}C$ increases to a maximum value of about 3‰. Values begin to decrease from 136 Ma and reach background values at about 132 Ma. The rate of change of $\delta^{13}C$ for the onset of the event (about 1.5‰/m.y.) is greater than for the decay (about 0.5‰/m.y.), suggesting an abrupt perturbation of the carbon system from equilibrium, followed by a more gradual return to background values.

1. Introduction

The correlation of Early Cretaceous calcareous nannofossil events to polarity chrons has been established by replicating this correlation in numerous Italian pelagic limestone sections [2–5]. The combination of magnetostratigraphy and nannofossil biostratigraphy now provides a practical integrated stratigraphic tool for Lower Cretaceous pelagic limestones in Italy, and similar sediments of this age elsewhere [6,7]. The nannofossil events aid the identification of polarity chrons and the resulting magnetostratigraphy provides the detailed stratigraphic control not available from nannofossil biostratigraphy alone. In this paper, the integrated stratigraphic approach is used to evaluate the synchroneity and timing of the Late Valanginian carbon isotope event, which has been observed in Italian pelagic limestone sections [8,9] and deep-sea cores [10]. As in previous papers [3–5], polarity chrons are numbered according to the correlative M-sequence oceanic anomaly, with the prefix 'C' to distinguish the chron (time interval) from the oceanic anomaly. Numbered oceanic magnetic anomalies usually correlate to reversed polarity chrons. Intervening normal polarity chrons are given the number of the next (older) reveresed chron with 'n' appended.

Carbon isotope geochemistry provides a tracer which can be used to monitor past global environmental conditions [11–18]. The Cretaceous is characterized by a number of positive carbon isotope events observed in whole-rock studies of pelagic limestones [11,12,18]. The best studied positive carbon isotope events in the Cretaceous time interval are at the Cenomanian–Turonian boundary [13–15], in the Aptian [8,11,16] and in

the Late Valanginian [9]. Another well-studied carbon isotope event occurs during the mid-Miocene [19]. These globally recognized $\delta^{13}C$ anomalies, which reflect repeated perturbations of the global carbon cycle, have duration of a few million years and peak $\delta^{13}C$ values 1–2‰ above pre-excursion values.

Carbon isotope events generally coincide with stratigraphic evidence for increased organic carbon burial, although this coincidence is more subtle for the Late Valanginian event. The presence of black shales in the Aptian and at the Cenomanian–Turonian boundary has led to these events being referred to as 'oceanic anoxic events' in the Cretaceous of the Atlantic and Tethyan realms. Fluctuations in the carbon isotope record can be explained by varying export rates of organic carbon from the atmospheric and oceanic reservoirs to the sedimentary reservoir. Positive $\delta^{13}C$ events result from an increase in the burial ratio of organic carbon to carbonate in marine sediments. The trigger for these short (a few million years) carbon burial events remains enigmatic. The major positive $\delta^{13}C$ events mentioned above seem to coincide with times of increased deposition of phosphate-rich sediments (e.g., the mid-Miocene Monterey Formation), thus suggesting a coupling between anomalies in the carbon and phosphorous cycles [20]. Within available age constraints, the $\delta^{13}C$ events appear to correlate with sea-level highstands and increased global volcanic activity.

A number of mechanisms, such as climate warming, increased biogenic productivity and changes in oceanic circulation patterns (e.g., oceanic stratification) have been invoked to link volcanic activity and/or sea-level rise to viable triggers for enhanced organic carbon burial and the observed $\delta^{13}C$ excursions. Some authors cite increased primary productivity stimulated by climate change as the primary cause of increased carbon burial. The Aptian and Late Valanginian $\delta^{13}C$ events have been postulated as being due to accelerated carbon cycling triggered by elevated atmospheric CO_2 levels coupled with a warm and humid climate [8,9]. These episodes of greenhouse climate conditions may be related to increased CO_2 emissions caused by intensified volcanic activity [21]. Enhanced continental weathering combined with increased runoff may have led to elevated transfer rates of nutrients to the oceans, favoring primary productivity and enhancing rates of biological carbon storage in the oceans. For the deposition of the mid-Cretaceous rhythmic black shales, it is generally more popular to invoke oceanic stratification and poor oceanic circulation (linked to sea-level rise or climate change) as the primary cause for the enhanced preservation of organic carbon [22–24]. According to the model proposed by Schlanger and Jenkyns [25] and Arthur et al. [14] for the Cenomanian–Turonian carbon isotope event, a major rise in global sea level resulted in flooding of expanded shelf areas, leading to increased surface water productivity and expansion of the mid-water oxygen-minimum zone which favored organic carbon preservation. These authors therefore invoked sea-level fluctuations as the driving force for changing organic carbon burial rates. Models involving marine transgressions causing changes in surface productivity and burial rate of organic carbon on shallow continental shelves have also been proposed to explain the mid-Miocene positive carbon isotope excursion [19].

The Late Valanginian carbon isotope event can be calibrated using magnetostratigraphy, whereas such age control is not available for the Aptian and Cenomanian–Turonian $\delta^{13}C$ events which are within the Cretaceous long normal polarity interval. In this paper, we present new isotope and magneto- and biostratigraphies from three Maiolica sections (Breggia, Pusiano and Val del Mis). We use previously published isotope and magneto- and biostratigraphies from Polaveno [5,9] and Capriolo [3,9] together with additional isotope data from these two localities. The magnetostratigraphies are used to produce age models for the isotope event at all five sections. Comparison of the isotope anomaly in different sections and assessment of rates of change of $\delta^{13}C$ may provide constraints on genetic models for Cretaceous carbon isotope/burial events.

2. Geological setting

The Mesozoic continental margin sediments exposed in the Southern Alps record the Jurassic and Cretaceous subsidence history of this part of the southern Tethyan continental margin since its

Liassic inception [26]. The Tithonian to Aptian interval is represented by the Maiolica Formation, which is a regularly bedded white/gray cherty pelagic limestone [27,28]. The formation is well exposed throughout the Southern Alps (Northern Italy) and the Umbria–Marche Basin (Central Italy). Similar coeval facies have been drilled in the Atlantic and Pacific oceans. Although the Maiolica in the Southern Alps shows rather abrupt thickness variations, from a few meters to over 300 m, the formation blankets both the structural high (Trento Plateau) and the intervening basins (Lombardian and Belluno basins) which characterized this part of the continental margin (Fig. 1). In the more complete sections, the contacts with the overlying Scaglia marly limestones and the underlying Rosso ad Aptici/Ammonitico Rosso are transitional. The biostratigraphic framework in the Maiolica Formation is derived from calcareous nannofossils, with additional control from calpionnellids in the Tithonian–Valanginian, and planktonic foraminifera in the Barremian–Aptian.

Of the five Maiolica sections discussed in this paper, four are located in the Lombardian Basin and one in the Belluno Basin (Fig. 1). All five sections are in Italy, apart from the Breggia section which is located in Switzerland, a few kilometers from the Italian border. Previously published section descriptions are available for Capriolo [3], Polaveno [5,29] and part of Breggia [9].

The Breggia section is located in the abandoned limestone quarry on the Breggia River close to the village of Balerna (Switzerland), 3 km northwest of Chiasso. The strata dip at about 50° to the southwest. Although the entire Maiolica

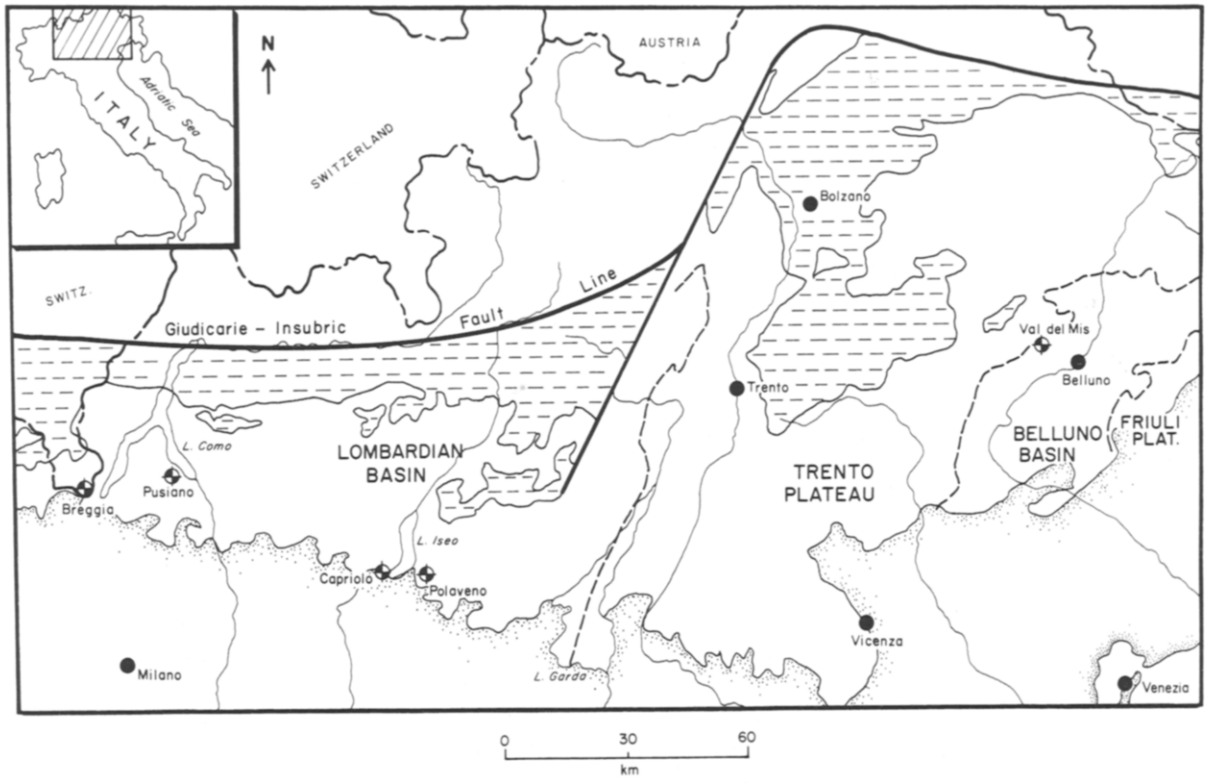

Fig. 1. Location map for Breggia, Pusiano, Capriolo, Polaveno and Val del Mis. Stippled area = limit of Quaternary sediments of the Po Plain. Horizontal dash ornament = predominantly igneous and metamorphic rocks. Area without ornament south of the Giudicarie–Insubric Line = predominantly Permian and Mesozoic sediments. Dashed lines = approximate limits of Mesozoic paleogeographic zones (Friuli Platform, Belluno Basin, Trento Plateau and Lombardian Basin). The Italian border with Switzerland and Austria is shown passing close to the Breggia section.

from its basal contact with the siliceous Rosso ad Aptici to the upper contact with the overlying Scaglia marlstones (total thickness 134 m) is exposed on the banks of the river on the southeast side of the quarry, the uppermost Barremian part is not easily accessible at the river and was sampled on the wall on the northwest side of the quarry. The Breggia section is therefore divided into two parts, referred to as the 'river' and 'wall' sections. The base (0 m level) of the river section is arbitrarily located 38 m above the base of the Maiolica, 17.7 m above a prominent interval of slumping. The total thickness of the river section is 70 m. The lower portion of this section consists of white to gray limestones with gray and black chert in nodules, lenses and layers. Bedding thicknesses of the limestones range from 10 to 30 cm. Common radiolarian-rich layers and thin pelitic joints are present. Between 23 m and 33 m, thin bedded gray limestones alternate with frequent, dark gray to black, 1–5 cm thick shales. Gray, marly limestones with gray to black chert occur between 33 and 64 m. The uppermost 6 m consist of light gray limestones and dark gray to black, 1–4 cm thick, layers of marlstones and claystones. Submarine slumped intervals were recognized at 9–14 m, 29 m, 38 m, 53 m and 64 m.

There is a sampling gap estimated to be about 1.5 m wide between the top of the river section and the base of the wall section. The wall section has a total thickness of 25 m and the top is marked by an abrupt lithological break between the Maiolica limestones and the overlying Scaglia marlstones. The lower 6 m of the measured section consist of thick bedded limestones with centimeter-thick chert nodules. A prominent reddish interval characterized by pseudonodularity occurs at 2.4–3.5 m. This peculiar interval has been observed in other Southern Alpine Maiolica sections too (Val del Mis (see below) and Cismon [30]) and is useful for lithostratigraphic correlation. From 6.3 m upwards, 5–10 cm thick black shales alternate with light gray limestones.

The Val del Mis section is located along the *arroyo* (watercourse) north of the bridge at the village of Mis, 10 km west of Belluno (Fig. 1). An adjacent section on the road north of Sospirolo along the west side of Lago di Mis, referred to as 'Valle del Mis' [31], is largely stratigraphically below the section discussed here, although the 'Valle del Mis' section studied recently by Tarduno [32] is correlatable with the 60–75 m interval of the section discussed here. The base of our measured section is located at a prominent fault. The strata dip at about 80° to the south-southeast. The lower part of the section comprises gray, well-bedded limestones with gray to black chert in nodules and layers. A reddish interval, correlative to the reddish interval at Breggia, occurs in the 43–52 m interval above the base. From 59 m upwards, 3–5 cm thick black shales alternate with gray limestones. The top of the Maiolica is at 92.60 m above the base of the measured section, at the contact with 85 cm of red nodular limestone yielding calcareous nannofossils of Late Albian age (see below). Red Cenomanian Scaglia overlies the Upper Albian limestones. VandenBerg and Wonders [33] attributed a 20 m stratigraphic interval in the top part of our measured section to the *B. breggiensis* Zone of the Albian, and resolved two reversed polarity zones which they attributed to short polarity chrons within the Cretaceous normal superchron. The revised biostratigraphy for this interval has indicated that only 85 cm of the section can be attributed to the Albian, and that this interval is bounded by unconformities which separate the Albian limestones from Barremian Maiolica below and Cenomanian limestones above.

The Pusiano section, located 10 km southwest of Lecco (Fig. 1), was sampled in a closed abandoned quarry on the west side of the road leading north from the village of Pusiano to the presently active limestone quarry. A stratigraphic thickness of 110 m was sampled on the eastern side of the quarry. The beds are vertical and occassionally slightly overturned; the youngest exposed strata outcrop at the southern end of this quarry face. The lower 50 m of the section consists of white to light gray limestones with gray to black chert in nodules, lenses and layers. Frequent radiolarian-rich layers are present. The interval between 50 and 58 m is characterized by dark gray to black, 3–10 cm thick shales alternating with dark gray, thin bedded limestones. Between 58 and 93 m, gray limestones alternate with marlstones. The upper 15 m consists of gray limestones with frequent, 3–8 cm thick, gray marlstones and claystones.

3. Carbon isotope stratigraphy

Carbon isotope data from Capriolo and Polaveno have been previously published [9]. In this paper, these data have been augmented and the entire isotope dataset has been correlated to previously published biostratigraphies and magnetostratigraphies [3,5]. The new isotope data from the Pusiano, Breggia and Val del Mis sections were acquired using the same methods [9], on splits from the samples used for biostratigraphy and magnetostratigraphy. The isotopic composition of carbonate was determined by analysis of CO_2 released by reaction of powdered bulk samples with 100% phosphoric acid at 50°C. The samples were roasted at 400°C prior to acid treatment in order to remove organic matter. The $\delta^{13}C$ composition of the CO_2 was determined

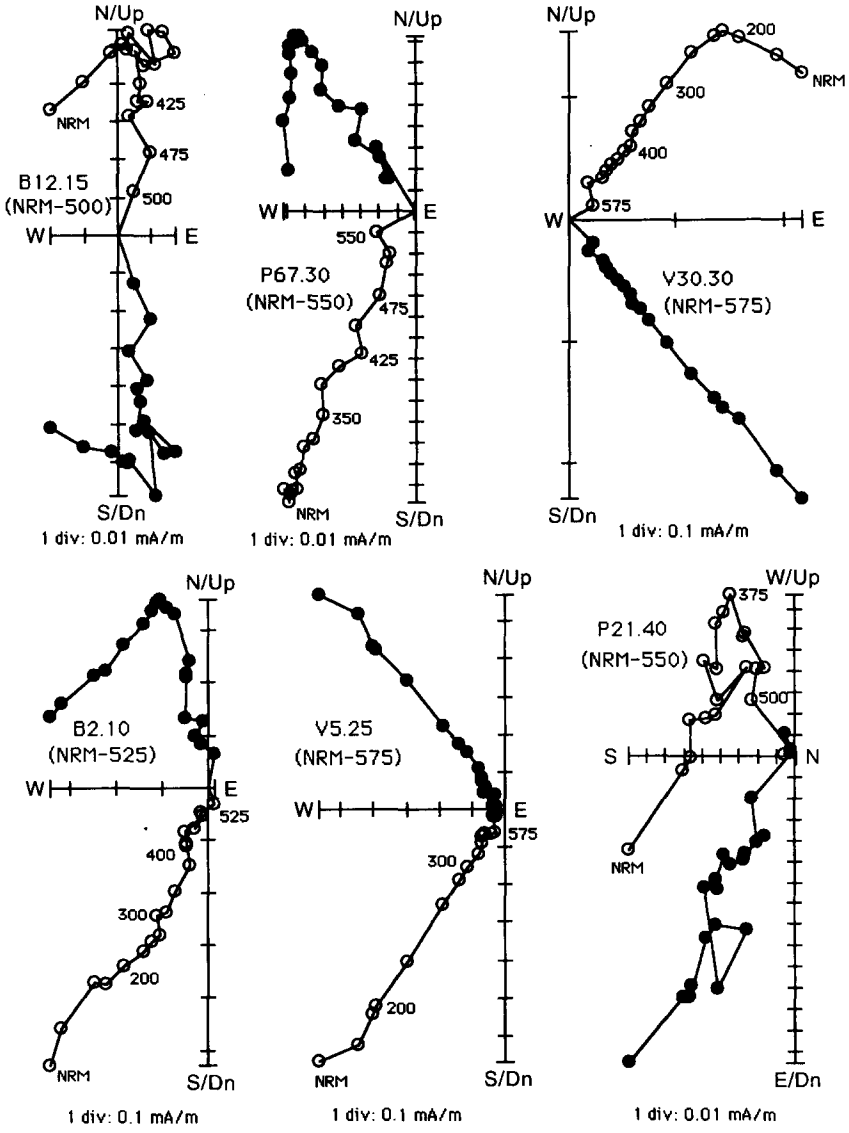

Fig. 2. Orthogonal projection of thermal demagnetization data for samples from Breggia (wall section) (prefix B), for Pusiano (prefix P) and for Val del Mis (prefix V). The meter level of the sample and the demagnetization temperature range is indicated. Temperatures associated with some individual points are given in degrees Celsius. Open and closed symbols represent projection of the vector end point of the magnetization vector on the vertical and horizontal planes, respectively.

using a triple collecting VG Micromass-903 mass spectrometer and the results are reported relative to the PDB (Pee Dee Belemnite) international isotopic standard. Replicate analyses of selected samples showed a reproducibility of better than 0.1%. The lack of covariance of $\delta^{13}C$ and $\delta^{18}O$ among samples of Maiolica limestones from Northern Italy [9] suggest that the $\delta^{13}C$ values have not been significantly altered by burial diagenesis. This conclusion is strengthened by the results of this paper which confirm the synchroneity of the isotope event in the various sections.

4. Magnetostratigraphy

Magnetostratigraphies for Polaveno [5] and Capriolo [3] have been previously published too. At, Pusiano, Breggia and Val del Mis oriented samples were collected in the field using a gasoline-powered hand-held drill. Stratigraphic spacing between the samples was generally about 50 cm. Each sample was treated by progressive thermal demagnetization in 25°C or 50°C steps until the magnetic moment of the sample decreased to the magnetometer noise level. The demagnetization range in which the characteristic magnetization component was resolved was determined (by eye) from orthogonal projections of the demagnetization data (Fig. 2), and the component direction was computed using the standard least squares method [34]. Component directions were then combined for each section using Fisher [35] statistics (Table 1 and Fig. 3). The maximum blocking temperatures are below 580°C (Fig. 2), consistent with previous work indicating magnetite as the remanence carrier in the Maiolica limestones [e.g., 3,5,30–32,36].

The virtual geomagnetic polar (VGP) latitude is a useful measure of polarity of the remanent magnetization. The VGP latitude for an individual sample magnetization is the latitude of the individual pole relative to the paleomagnetic pole for the entire section computed from the section mean direction. VGP latitudes were computed from sample component directions and the resulting VGP latitude distribution interpreted in terms of polarity zones (Figs. 4–9). The resulting polarity pattern in these sections is usually not sufficiently distinctive for unequivocal correlation to the polarity timescale. However, this correlation can be made with the aid of the nannofossil biostratigraphy, using established correlations of polarity chrons to nannofossil events [2–5].

For the Capriolo and Polaveno sections, we adopt the previously published magnetostratigra-

TABLE 1

Mean directions of the characteristic magnetization for each section, before and after structural tilt correction

	Before tilt correction					After tilt correction			
	N	Dec.	Inc.	k	α_{95}	Dec.	Inc.	k	α_{95}
Breggia (wall section)	76	8.1	1.0	29.5	3.0	351.1	41.2	28.6	3.1
Breggia (river section)	100	10.3	0.4	9.2	4.9	350.2	41.0	7.6	5.5
Pusiano	185	322.8	-43.3	5.1	5.1	326.7	47.8	4.7	5.4
Val del Mis	158	311.6	-40.7	5.0	5.6	310.4	30.1	12.4	3.3
Polaveno [5]	367	332.8	20.2	24.5	1.5	322.0	36.1	24.6	1.5
Capriolo* [36]	137	328.7	65.6	7.2	4.8	321.4	38.4	7.2	4.8

POLES	Lat °N	Long °E	dp	dm
Breggia (wall)	66.7	210.0	2.3	3.8
Breggia (river)	66.3	211.9	4.0	6.7
Pusiano	59.0	258.1	4.6	7.0
Val del Mis	39.2	262.8	2.0	3.7
Polaveno [5]	49.7	253.5	1.0	1.7
Capriolo* [36]	50.5	255.6	3.4	5.7

* Hauterivian–Barremian only. Statistical parameters after Fisher [35]

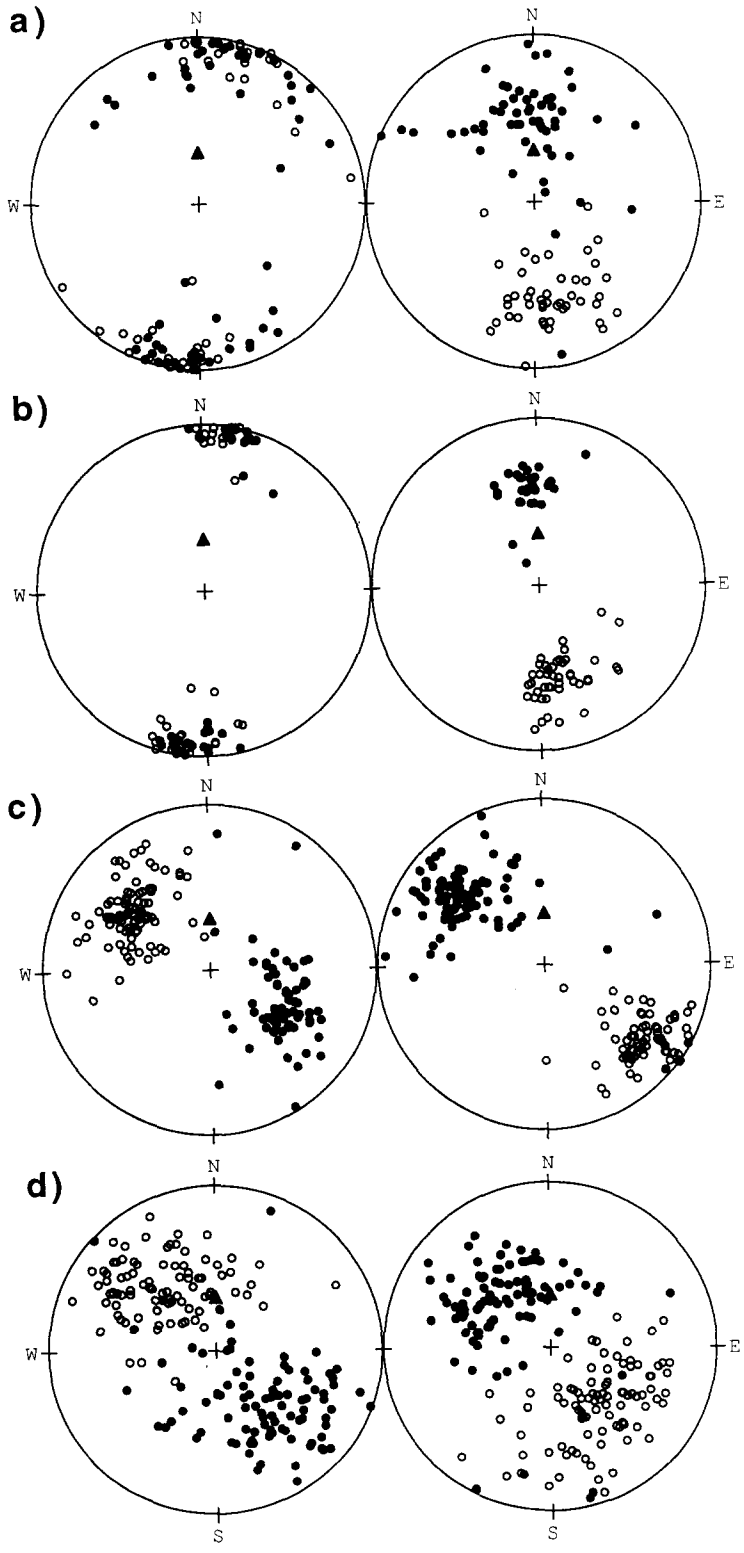

Fig. 3. Equal-area projection of characteristic magnetization components before (left) and after (right) structural tilt correction for (a) Breggia river section, (b) Breggia wall section, (c) Val del Mis and (d) Pusiano. Open and closed symbols represent upward and downward inclination, respectively. Triangle represents the present field direction at the sampling site.

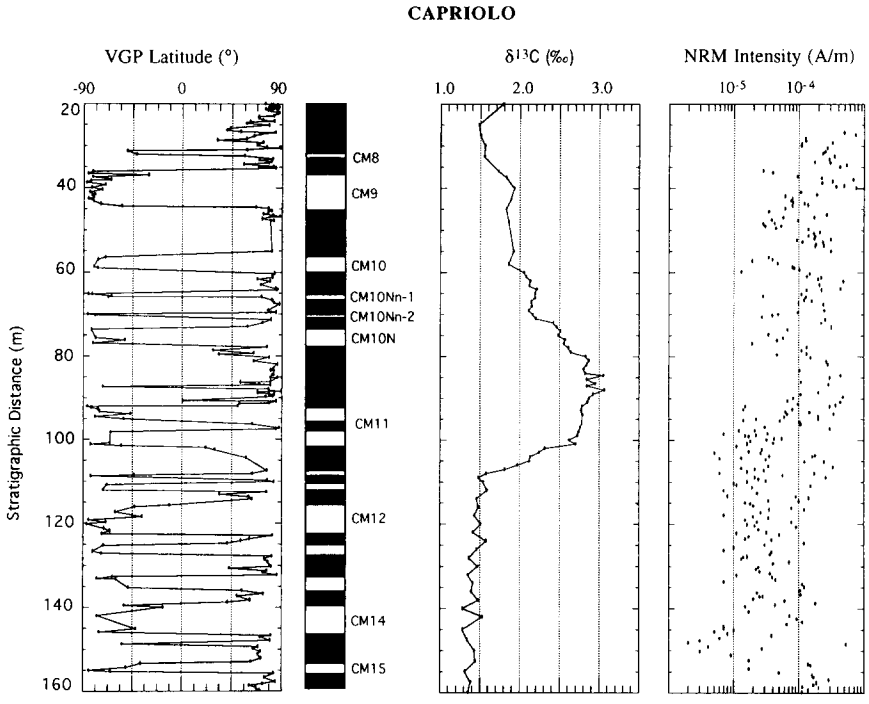

Fig. 4. Correlation of magnetostratigraphy, carbon isotope stratigraphy and NRM intensity at Capriolo [3,9].

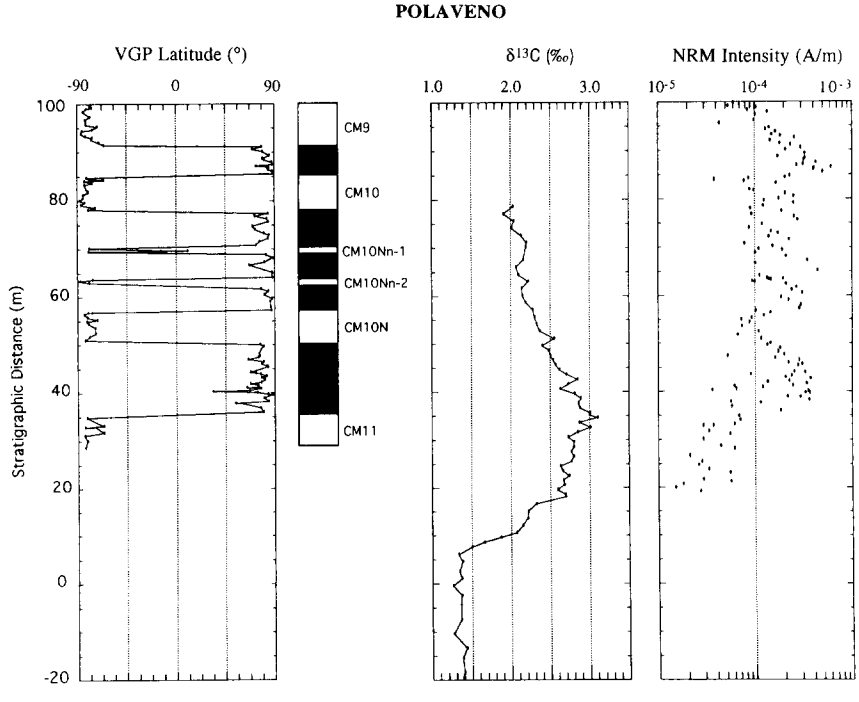

Fig. 5. Correlation of magnetostratigraphy, carbon isotope stratigraphy and NRM intensity at Polaveno [5,9].

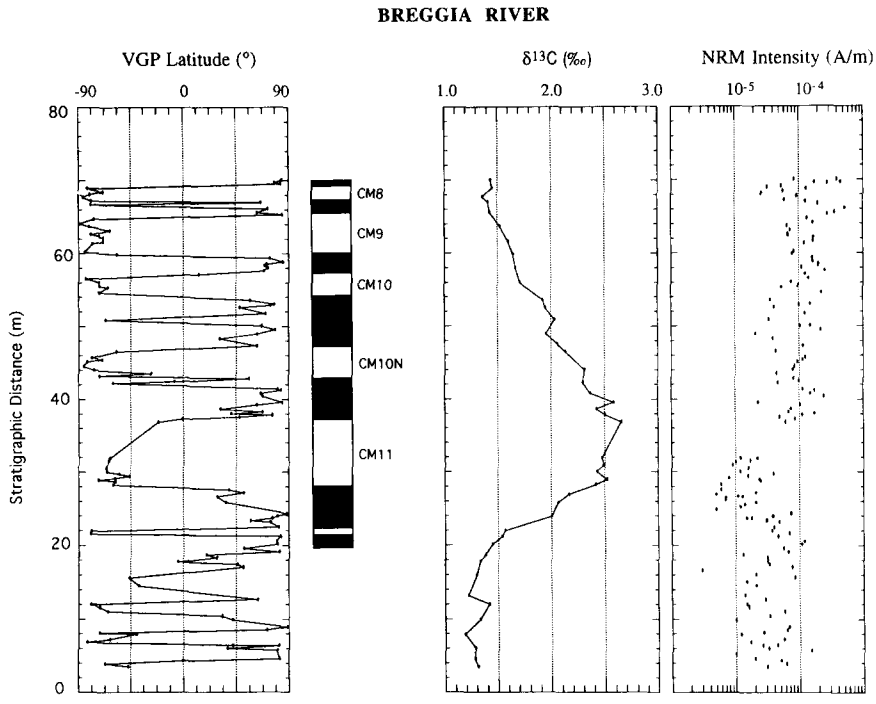

Fig. 6. Correlation of magnetostratigraphy, carbon isotope stratigraphy and NRM intensity for the river section at Breggia.

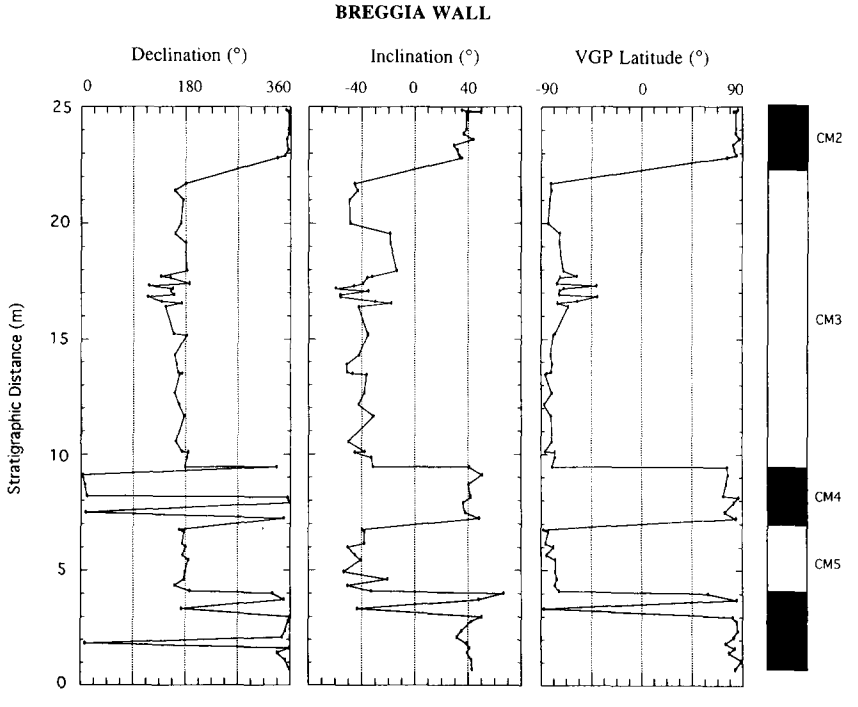

Fig. 7. Magnetization component declination and inclination, VGP latitudes and polarity chron interpretation for the wall section at Breggia.

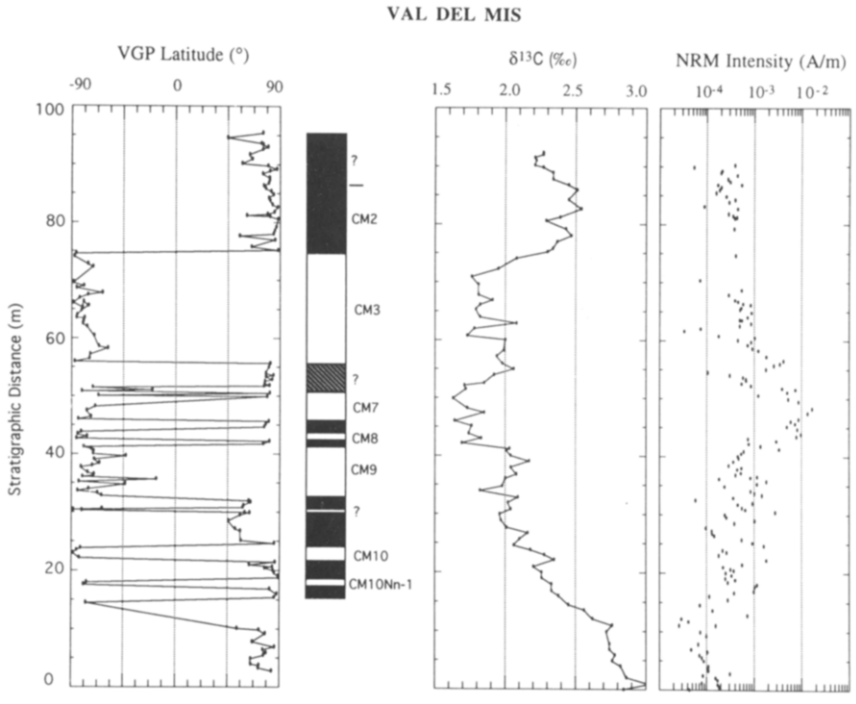

Fig. 8. Correlation of magnetostratigraphy, carbon isotope stratigraphy and NRM intensity at Val del Mis.

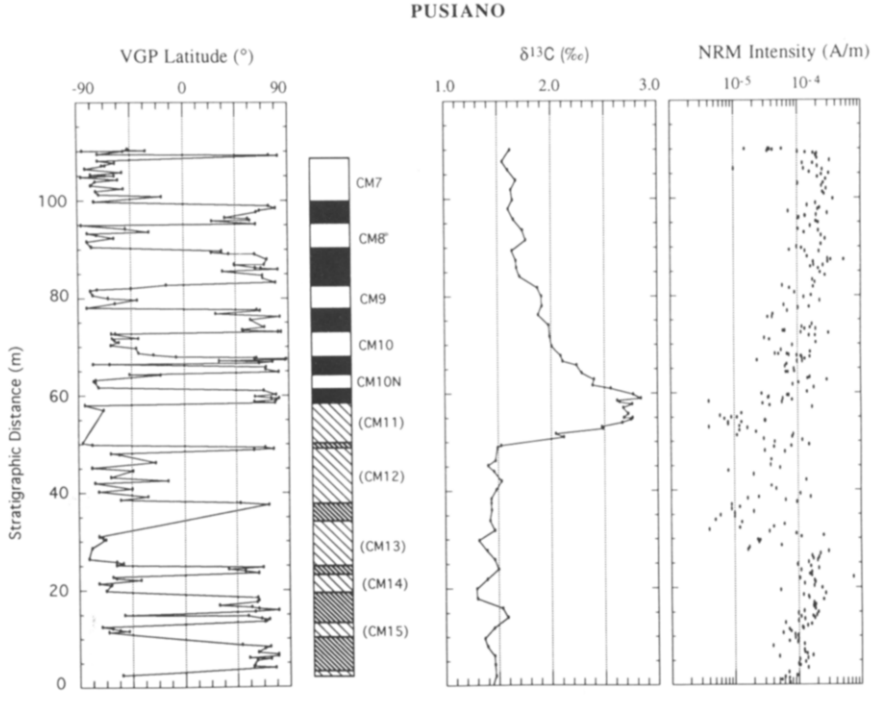

Fig. 9. Correlation of magnetostratigraphy, carbon isotope stratigraphy and NRM intensity at Pusiano. The hatching in the polarity column indicates tentative chron designation.

phies [3,5] and carbon isotope stratigraphies [9] (Figs. 4 and 5). The magnetostratigraphy at Polaveno (Fig. 5) does not cover the entire interval recording the isotope event as the intensity of the natural remanent magnetization (NRM) decreases to values below magnetometer noise level close to the peak $\delta^{13}C$ values. A similar decrease in NRM intensity is observed at Capriolo (Fig. 4), but here the NRM intensities were sufficiently high for the magnetostratigraphy to be resolved throughout the $\delta^{13}C$ event.

As mentioned above, the Breggia section is subdivided into two parts. There is no overlap between the river section (Fig. 6) and the wall section (Fig. 7) and there is a sampling gap of about 1.5 m between them. The river section yielded a VGP latitude distribution which can be interpreted in terms of polarity zones only above the 20 m level (Fig. 6). The labeling of polarity chrons is aided by the location of nannofossil events (see below). A decrease in NRM intensity (similar to that seen at Capriolo and Polaveno), at and below the peak value of $\delta^{13}C$, results in poor resolution of magnetization components below 20 m and an uninterpretable VGP latitude distribution. For the wall section (Fig. 7), the VGP latitudes can be interpreted as chrons CM2–CM5 on the basis of polarity pattern fit and the position of nannofossil events characteristic of this interval (see below). The poor definition of the base of CM5 in the wall section (Fig. 7) is attributed to the 1 m thick reddened interval (at 2.30–3.40 m), which is a condensed hematite-bearing interval which can be correlated to other Southern Alpine sections.

At Val del Mis, the VGP latitudes indicate a clear distribution of polarity zones, apart from in the 48–52 m interval (Fig. 8). This is within the reddened condensed interval which is at approximately the same stratigraphic level as the reddened interval at Breggia. Above and below this condensed interval the polarity zones can be interpreted and labeled in terms of polarity chrons, with the aid of the nannofossil stratigraphy. The polarity zone pattern indicates that sedimentation rates were very variable in this section. Only the young part (decay) of the $\delta^{13}C$ event is recorded in this section. Again, the NRM intensity decreases towards the peak in $\delta^{13}C$ at the base of the measured section.

At Pusiano, the distribution of VGP latitudes indicates a clear pattern of polarity zones above 60 m (Fig. 9). In the 30–60 m interval, the magnetization components are poorly defined due to the low NRM intensities and some samples did not yield magnetization components. The resulting low density of VGP latitudes in this interval inhibits the definition of polarity zones. With the aid of the nannofossil events, the polarity zones are correlated to M-sequence chrons, although chron boundaries in the 30–60 m interval remain poorly defined.

It is of interest to note that the top of the Maiolica Formation at Val del Mis and Breggia is in a polarity zone correlative to CM2 whereas the top of the Maiolica at Capriolo and Pie' del Dosso (near Polaveno) was deposited in CM0n [5]. This difference of about 6 m.y. in the age of the top of the Maiolica in adjacent sections can probably be best explained in terms of variable ocean-floor erosion prior to the deposition of the overlying Scaglia marlstones.

Mean magnetization directions and pole positions for Polaveno, Capriolo and Pusiano (Table 1) are consistent with recently compiled Southern Alpine paleomagnetic data of Hauterivian–Barremian age [36]. At Val del Mis, both the mean inclination and declination have slightly lower values than those observed in Southern Alpine sections of comparable age [36]. This may indicate inadequate structural tilt correction at this site and/or about 12° anticlockwise rotation of the Val del Mis section relative to other Southern Alpine sections. The Breggia sections have been rotated clockwise by about 25° relative to other Southern Alpine sections for which data are available.

5. Biostratigraphy

The Early Cretaceous nannofossil zonation of Thierstein [37,38] has been shown to be useful for stratigraphic subdivision of the Maiolica limestones in Italy [2–5]. Although in the Maiolica nannofossil preservation is compromised by diagenetic dissolution and overgrowth, the key nannofossil events consistently correlate to particular polarity chrons in Southern Alpine and Umbrian sections [2–5]. Thierstein's zonation has been replicated in several low-latitude outcrop and

oceanic sites, although a few marker species with a spotty distribution have been reported at different stratigraphic levels in different oceans. In this paper, we use the standard events proposed by Thierstein [37,38] for the definition of zonal boundaries as well as additional datums which consistently correlate to particular polarity chrons in Italian pelagic limestone sections [2–5].

Biostratigraphic data from Polaveno [5] and Capriolo [3] have been previously published. Preliminary nannofossil biozonations for the Breggia river section have also been previously presented [9,39] and correlated to isotope stratigraphy [9].

Splits from the samples studied for magnetostratigraphy and isotopes were used for biostratigraphic study at Breggia, Pusiano and Val del Mis. Following the standard technique [40], smear slides were prepared with Canada Balsam and studied using a light polarizing microscope at 1250 × magnification. Total and species abundances were semi-quantitatively estimated following the methods of Erba and Quadrio [29]. The poor to moderate preservation and low abundance of marker species required the observation of several hundred fields of view for each sample. Despite the low abundance of marker species, the species ranges for each section are often continuous, allowing the first (FAD) and last (LAD) appearance datums to be determined fairly precisely (Figs. 10–13). The meter level of FADs and LADs are reported as lowest (oldest) sample (FAD) and uppermost (youngest) sample (LAD) in which the marker species was observed. The meter level in parentheses in Table 2 is the level of the sample immediately below the FADs or immediately above the LADs, indicating the stratigraphic uncertainity of the datums.

Calcareous nannofossils are common and moderately to poorly preserved in the Breggia river section (Fig. 10). *Calcicalathina oblongata*

TABLE 2

Nannofossil events and reversed polarity chrons

Nannofossil events	Reversed polarity chrons	Breggia (m)	Pusiano (m)	Val del Mis (m)
	End CM3	22.25 (wall)		74.90
LAD *C. oblongata*		10.00 (10.20)		58.25 (59.20)
	Begin CM3	9.45		55.80
LAD *L. bollii*		7.00		
	End CM5	7.50 (7.70)		50.52 (51.50)
	Begin CM5	4.05		
	End CM7			49.00
FAD *T. terebrodentarius*			102.38 (101.84)	47.45 (48.20)
	Begin CM7		99.00	45.80
	End CM8	69.20 (river)	95.05	44.20
LAD *C. cuvillieri*		67.00 (67.80)	90.48 (91.37)	43.00 (43.80)
	Begin CM8	66.40	90.10	42.35
	End CM9	65.00	82.90	41.45
	Begin CM9	59.60	77.80	32.40
	End CM10	56.80	72.90	24.25
	Begin CM10	54.10	67.85	21.80
FAD *L. bollii*		53.54 (53.00)	67.72 (67.46)	21.45 (20.45)
	End CM10Nn-1			18.40
	Begin CM10Nn-1			17.30
	End CM10Nn-2			14.95
	Begin CM10Nn-2			12.25
	End CM10N	46.90	64.60	
FAD *N. bucheri*		44.00 (43.00)	61.99 (61.30)	
	Begin CM10N	41.80	61.30	
	End CM11	37.00	58.25	
LAD *T. verenae*		37.80 (39.00)	54.91 (56.00)	0.01
	Begin CM11	27.85	49.60	
FAD *T. verenae*		16.00 (15.00)	53.91 (48.70)	
	End CM12		48.45	
	Begin CM12		38.20	
	End CM13		34.30	
FAD *C. oblongata*		3.50 (3.00)	25.10 (24.60)	
	Begin CM13		24.80	
	End CM14		23.15	
	Begin CM14		19.15	
	End CM15		12.99	
	Begin CM15		10.06	
FAD *C. angustiforatus*			4.44 (3.44)	
	End CM16		3.20	

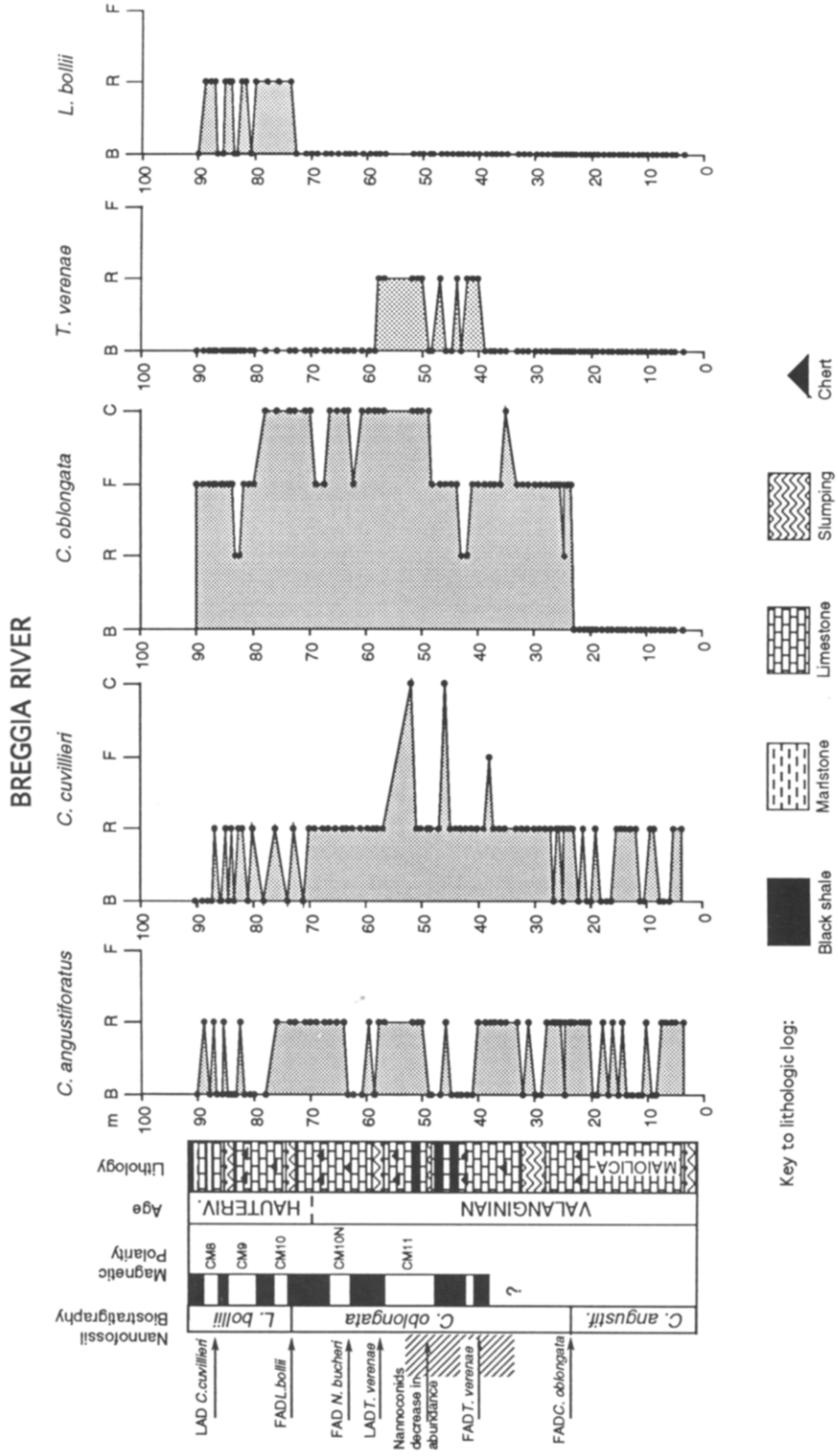

Fig. 10. Distribution of calcareous nannofossil marker species in the Breggia river section, with correlation to simplified lithological log and magnetostratigraphy. *B* = barren; *R* = rare; *F* = frequent; *C* = common.

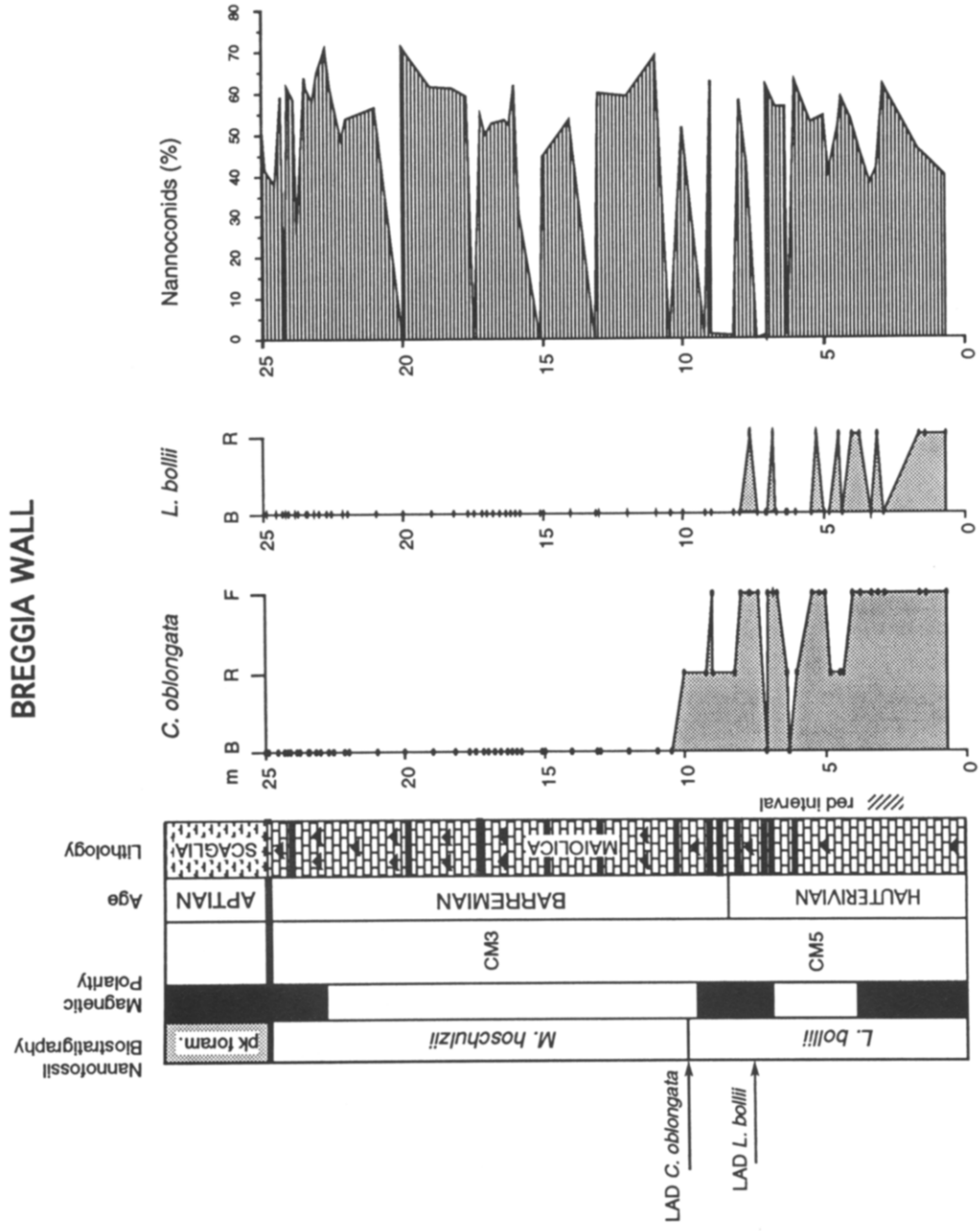

Fig. 11. Distribution of calcareous nannofossil marker species in the Breggia wall section, with correlation to simplified lithological log and magnetostratigraphy. For key to symbols, see Fig. 10.

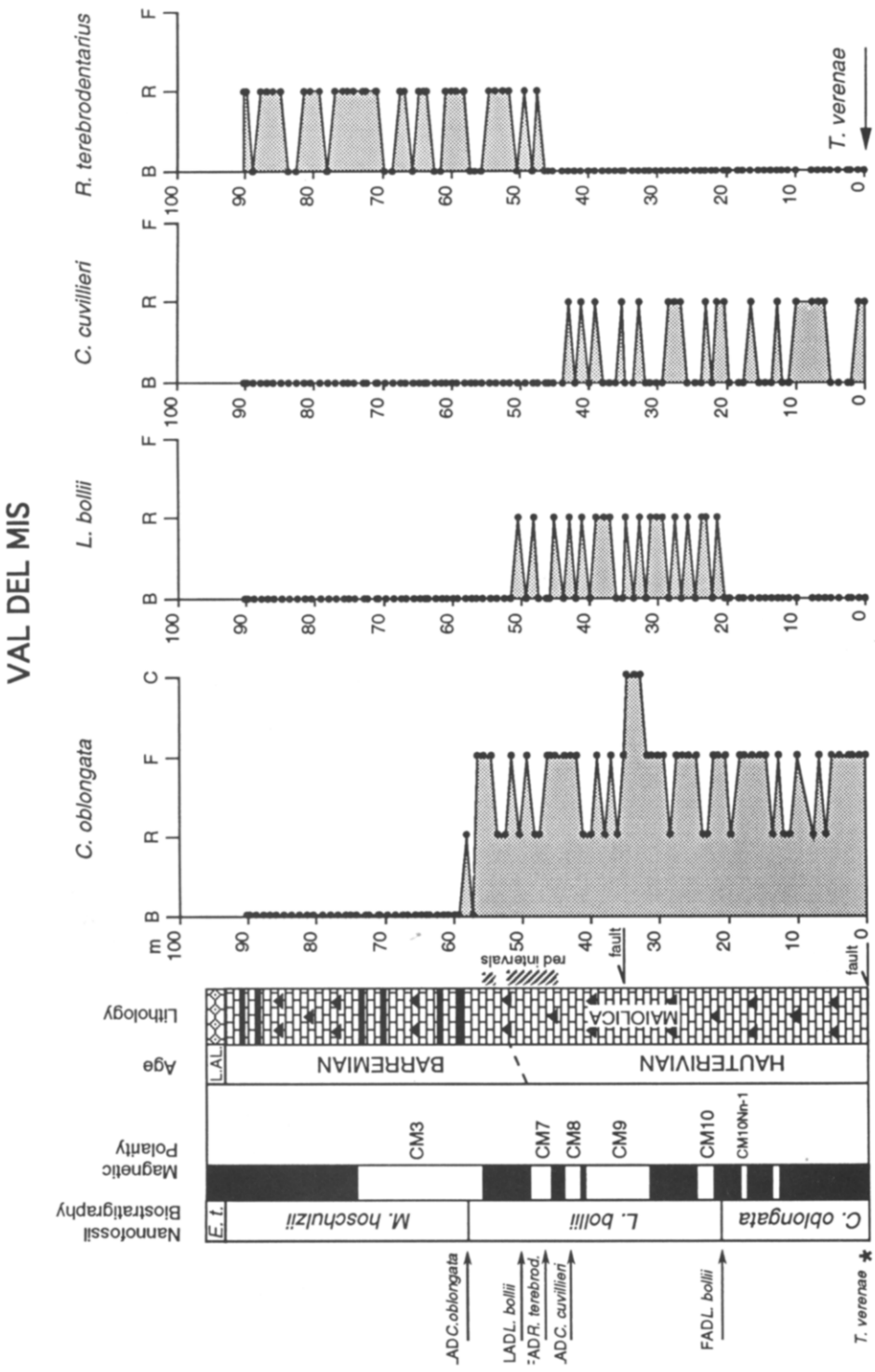

Fig. 12. Distribution of calcareous nannofossil marker species in the Val del Mis section, with correlation to simplified lithological log and magnetostratigraphy. For key to symbols, see Fig. 10.

was first observed at 3.50 m and is frequent to common throughout the section. The FAD of *C. oblongata* is correlated to the Early Valanginian [37,38] and to chron CM14 [3,41]. A sharp decrease in abundance of nannoconids was observed between 13 and 30 m. Below and above this interval they are the dominant forms. A similar pattern was also reported for the Capriolo and the Polaveno sections. At Capriolo nannoconids decrease in abundance between 100 and 130 m (interval comprising CM11 and CM12) [3], whereas at Polaveno a low abundance of nannoconids is reported between 90 and 120 m [29], in the interval immediately below CM11 [5]. The decrease in abundance of nannoconids is not considered an artifact of differential dissolution because these nannoliths are very resistant to diagenesis. Moreover, the synchronous decrease in abundance observed in different sections suggests primary changes in paleoceanographic conditions at least on a regional scale.

Only rare specimens of *Tubodiscus verenae* were observed in the Breggia river section, between 16.0 and 37.8 m, but the fairly continuous occurrence suggests that the FAD and LAD of this marker are reliable. Consistent with previous work [2,5], *T. verenae* is distinguished from *T. jurapelagicus*, which was observed in the interval between 6 and 16 m. The FAD and LAD of *T. verenae* are useful events in the Valanginian and occur below CM11N and CM10N, respectively. *Nannoconus bucheri* was first observed at 44 m, within CM10N. The first occurrence of *N. bucheri* is reported close to the base of CM10N at Capriolo [3] and at the base of CM10N at Polaveno [5,29]. At 37.8 and 52.2 m single specimens of *Rucinolithus wisei* were observed. This marker species, restricted to the Berriasian–Valanginian, is usually extremely rare [3] or absent [2,29] in Maiolica sections. The FAD of *Lithraphidites bollii*, dated to the Early Hauterivian and correlated to the base of CM10 [2,3,5], was recorded at 53.10 m. *Cruciellipsis cuvillieri* was not observed above 67.0 m. This species is rare in the upper part of its range as previously observed in other Maiolica sections [3,5,29]. The LAD of *C. cuvillieri*, dated to the Late Hauterivian, occurs within CM8 [2,3,5].

The limestones of the Breggia wall sections contain extremely abundant nannoconids that constitute up to 70% of the nannofloral assemblage. The nannoconids show rhythmic fluctuations in abundance, with minimum values corresponding to organic carbon rich black shales (Fig. 11). *Lithraphidites bollii* was observed in the bottom part of the section and the LAD is detected at 7.5 m, corresponding to the lower part of CM4. It should be noted that the distribution of this species is fairly continuous up to 5.3 m within CM5, whereas *L. bollii* was not observed in the upper part of CM5. Single specimens were detected in only two samples, from the top of CM5 and the lower part of CM4. A similar distribution was reported for the Polaveno section [5], where a single specimen of *L. bollii* in one sample from CM4 was interpreted as reworked. At other localities, the LAD of this marker species was correlated to CM5 [2,3] probably as a result of less detailed sampling. Following the stratigraphy of Thierstein [37,38], the LAD of *L. bollii* has been used as an Early Barremian event. Recent studies on the Gorgo Cerbara section of Central Italy [42] and the Caravaca section of Spain [Mutterlose and Erba, in prep.] revealed that the LAD of *L. bollii* occurs in the Angulicostata Ammonite Zone of Late Hauterivian age. The LAD of *Calcicalathina oblongata*, of Early Barremian age, occurs at 10.0 m in the lowermost part of CM3. The nannofloral assemblage remains very constant through the Maiolica in the wall section and none of the Late Barremian nannofossil events was recorded. The Scaglia marlstones overlying the top of the Maiolica limestones were dated using planktonic foraminifera [28]. A hiatus spanning the Late Barremian to Early Aptian was determined by the occurrence of the *Globigerinoides ferreolensis* zone at the base of the Scaglia.

Calcareous nannofossils are common and moderately to poorly preserved in the Val del Mis section. The distribution of marker species is reported in Fig. 12. Extremely rare specimens of *Tubodiscus verenae* were observed only in the bottom sample (0.01 m) and therefore we do not use this marker species for biostratigraphy in this section. *Nannoconus bucheri* is present from the base of the section. *Lithraphidites bollii* is present from 21.45 m to 50.52 m. As in the Breggia river section, the Early Hauterivian FAD of *L. bollii* (21.25 m) occurs slightly below the base of CM10. The LAD of *L.bollii* was detected at 50.52 m in

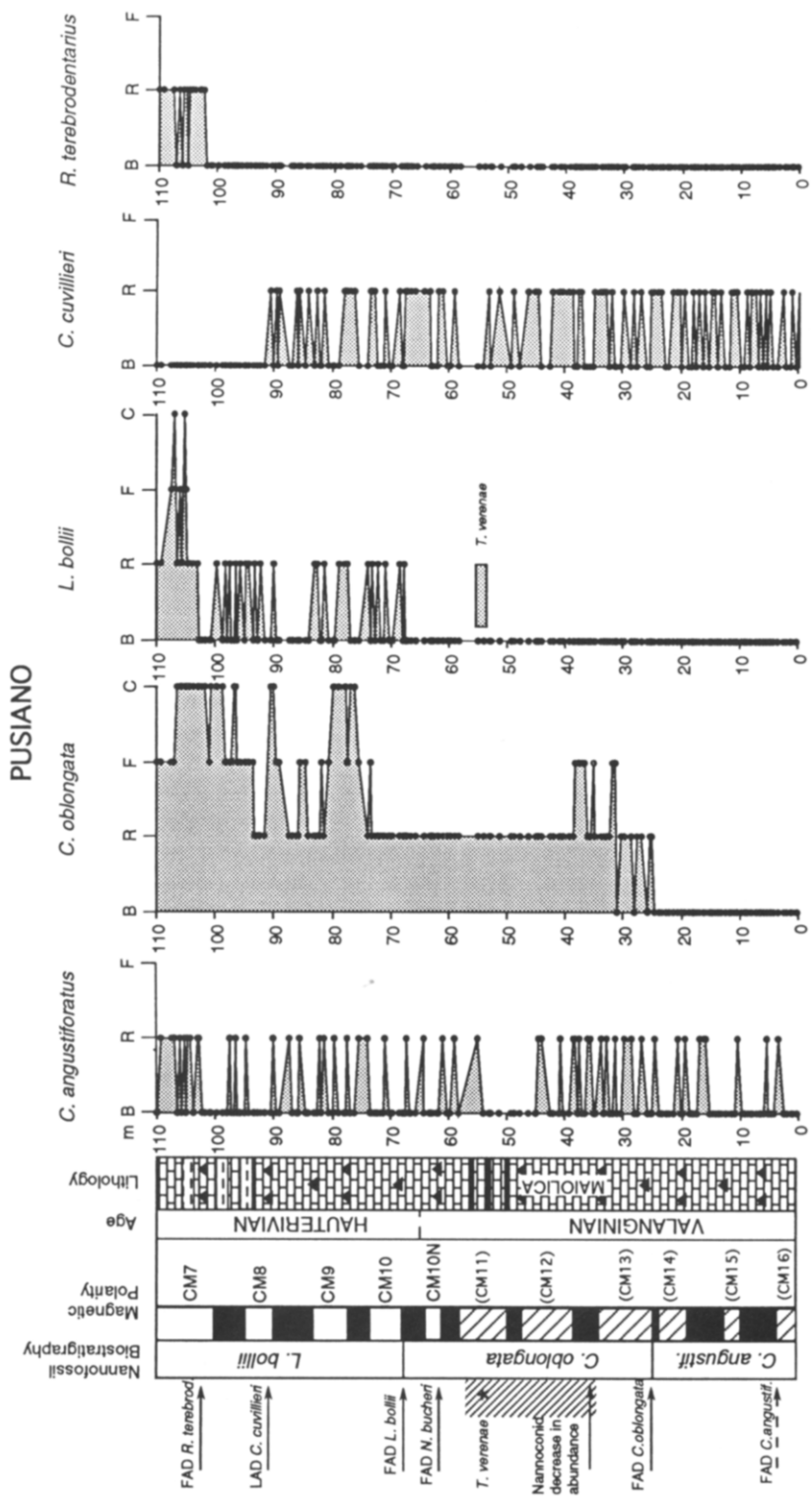

Fig. 13. Distribution of calcareous nannofossil marker species in the Pusiano section, with correlation to simplified lithological log and magnetostratigraphy. For key to symbols, see Fig. 10.

the reddish interval, with poor definition of polarity zones between CM7 and CM3 (see above). The LAD of *Cruciellipsis cuvillieri* occurs at 42.35 m, within CM8. *Rucinolithus terebrodentarius* was observed from 47.45 m upwards. Its FAD, used as a Late Hauterivian event, correlates with CM7. The LAD of *Calcicalathina oblongata* at 58.25 m falls in the lower part of CM3. As previously reported for the Breggia wall section, the remainder of the Barremian at the Val del Mis section is characterized by a very constant nannofloral assemblage dominated by nannoconids and none of the Late Barremian events were observed (see also paleontological data reported by Tarduno [32]). In the red nodular limestones overlying the Maiolica, the nannofossil assemblage is indicative of the *Eiffellithus turriseiffelii* Zone of Late Albian age. This implies a long hiatus of several million years. However, nannofossils are extremely dissolved in the hardground marking the lithological boundary between the Maiolica and the Scaglia formations. Only non-diagnostic, long-ranging species have been observed, and the presence of Aptian to Mid-Albian sediments cannot be ruled out.

In the Pusiano section (Fig. 13), calcareous nannofossil assemblages are very similar to those observed at Breggia and Val del Mis. *Cretarhab-*

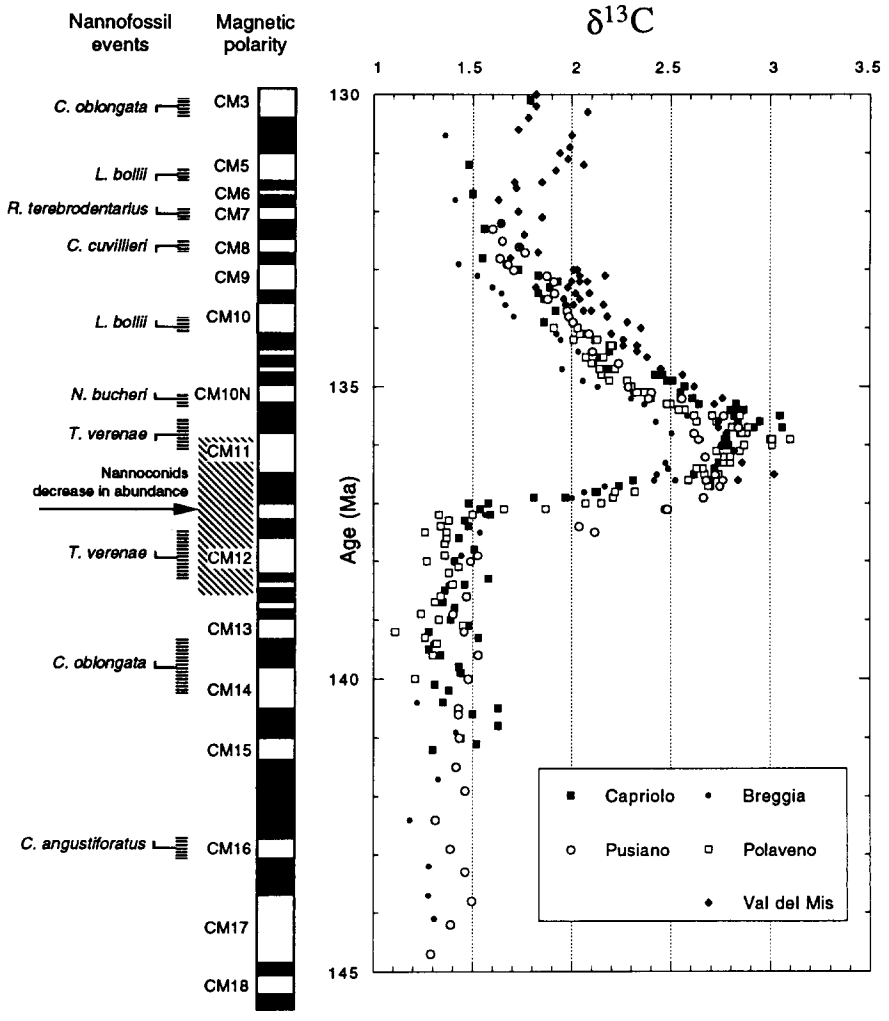

Fig. 14. Carbon isotope data for Capriolo, Breggia, Pusiano, Polaveno and Val del Mis correlated to absolute age by linear interpolation between magnetostratigraphically derived age/depth points using the GST89 timescale [1]. Correlations of polarity chrons and nannofossil events to the $\delta^{13}C$ event are shown.

dus angustiforatus is always rare and its FAD is tentatively placed at 4.44 m, within CM16, where this species was first observed. However, the discontinuous distribution of *C. angustiforatus* in the Pusiano section makes this event somewhat unreliable. The FAD of *Calcicalathina oblongata* occurs at 25.10 m, at the base of CM13, and this species is always present throughout the rest of the section. As previously reported for the Breggia river section, a marked decreased in abundance of nannoconids was observed in the interval comprising CM12 and CM11 (between 40 and 58 m). Rare specimens of *Tubodiscus verenae* were observed only at 53.91 and 54.91 m, within CM11. Therefore, this marker species was not used for biostratigraphy at Pusiano. *Nannoconus bucheri* was first observed at 61.99 m, at the base of CM10. *Lithraphidites bollii* is rare to common from 67.72 m upwards. The FAD of *L. bollii* slightly pre-dates the beginning of CM10 as previously reported for the Breggia river and Val del Mis sections. *Cruciellipsis cuvillieri* occurs up to 90.48 m and its LAD falls within CM8. The FAD of *Rucinolithus terebrodentarius* was detected within CM7, at 102.38 m.

The established correlation of nannofossil events to polarity chrons [2–5] aids the assignment of polarity chrons at Breggia, Val del Mis and Pusiano. The sequential occurrence of polarity chrons in the sections and the lack of conflicts with previous correlations of polarity chrons to nannofossil events serves to strengthen the established correlations of nannofossil datums with polarity chrons (Fig. 14). Two additional events, the FAD of *N. bucheri* and the decrease in the abundance of nannoconids, are proposed as new markers for the Late Valanginian–Early Hauterivian interval.

6. Age model

The age model for each section was constructed by assigning ages to polarity zone boundaries using the timescale of Harland et al. [1] and linear interpolation between age/depth control points. The number of control points depended on the number of identified polarity zones in each section and varied from 39 for Capriolo to 10 for Polaveno and Pusiano. The magnetostratigraphy at Polaveno does not cover the entire interval recording the $\delta^{13}C$ event (Fig. 5), due to an abrupt decrease in magnetization intensity coinciding with the $\delta^{13}C$ peak. For this section, the entire magnetostratigraphy records CM3 to CM11 and the sedimentation rate, by comparison to the oceanic anomaly record, was apparently very constant [5]. We therefore assume that sedimentation rate in the CM9 to CM11 interval at Polaveno (Fig. 5) can be extrapolated downsection through the interval recording the $\delta^{13}C$ event. At Val del Mis, only the decay of the $\delta^{13}C$ event is recorded (Fig. 7) and the age model is applied to only this part of the $\delta^{13}C$ record.

On applying the age model to all five sections, there is close replication of the $\delta^{13}C$ records plotted against absolute time (Fig. 14). Background values of $\delta^{13}C$ of 1.5‰ are recorded from 145 to 137 Ma. Between 137 and 136 Ma, $\delta^{13}C$ increases to a maximum value of about 3‰. Values begin to decrease at about 136 Ma and reach the background level of 1.5‰ at 132 Ma (Fig. 14). Using the Kent and Gradstein timescale [43], the increase in $\delta^{13}C$ occurs between 134 and 132.5 Ma, and values reach background values at about 127.5 Ma. We prefer the Harland et al. timescale [1] as it is consistent with the recent correlation of Ontong–Java volcanism at 123 Ma to the base of the Cretaceous Long Normal, at a time slightly post-CM0 [44].

7. Conclusions

Many studies have demonstrated that magnetite is the principal carrier of remanent magnetization in the Maiolica [e.g., 3,5,30–32]. A decrease in NRM intensity in the interval recording the $\delta^{13}C$ event was observed in all sections (Figs. 4–6, 8 and 9). There is no magneto- or biostratigraphic evidence for large changes in sedimentation rate coinciding with the $\delta^{13}C$ event, suggesting that carbonate accumulation variations are not controlling the NRM intensity. Diagenetic magnetite dissolution in this environment is probably controlled by the availability of sulfide which, in turn, is controlled by the availability of sulfate (from seawater) and by the activity of sulfate-reducing bacteria [45,46]. The bacterial activity will, in turn, be controlled by the availability and nature of buried organic matter. Although there are

no thick black shale horizons in the Maiolica coinciding with the Late Valanginian $\delta^{13}C$ event, the bedding is thinner in this interval and dark gray limestones alternate with many centimeter-thick dark gray to black shales which are not seen in the thicker bedded limestones above and below. The decrease in NRM intensity, coinciding with the $\delta^{13}C$ event and the increase in organic carbon burial, suggests that the availability of organic carbon which could be metabolized by sulfate-reducing bacteria was the limiting factor controlling magnetite dissolution in this pelagic environment.

The Late Valanginian carbon isotope anomaly peaks in chrons CM10N and CM11. The close replication of the $\delta^{13}C$ records plotted against absolute time (Fig. 14) indicates that the principal features of the $\delta^{13}C$ records from bulk carbonate in these pelagic limestones are not an artifact of sediment diagenesis but a synchronous paleoceanographic signal. We consider that the distance between the sampled sections (Fig. 1) precludes the possibility that the observed $\delta^{13}C$ records are due to selective diagenesis. The tight age control allows the rates of change of $\delta^{13}C$ to be estimated. The onset of the $\delta^{13}C$ event indicates a rate of change of $\delta^{13}C$ of about 1.5‰/m.y. The $\delta^{13}C$ peak lasts for about 1 m.y. and the event decays at a rate of about 0.5‰/m.y. The amplitudes of the Cenomanian–Turonian and Late Valanginian $\delta^{13}C$ events are comparable; however, the rates of change of $\delta^{13}C$ during the onset and decay of the Cenomanian–Turonian event were estimated to be comparable (1–2‰/m.y.) [13,14]. The high estimated $\delta^{13}C$ decay rate at the Cenomanian–Turonian boundary was considered to imply an increase in rate of supply of isotopically light carbon to the ocean during the decay of the event, rather than a simple decrease in the rate of organic carbon burial. This could have been accomplished through recycling of previously deposited organic carbon by erosion and/or oxidation [14]. The more gradual $\delta^{13}C$ decay rate for the Late Valanginian event (0.5‰/m.y.) implies a different mechanism for the re-establishment of pre-excursion $\delta^{13}C$ values, and emphasizes the importance of accurate estimates of the rate of change of $\delta^{13}C$.

The offlap and onlap geometry from seismic stratigraphy has been interpreted to indicate that the Late Valanginian was a time of sea-level rise, with a sea-level highstand in chron CM10N [47], coinciding with the $\delta^{13}C$ peak. The Early Aptian, Cenomanian–Turonian and mid-Miocene $\delta^{13}C$ peaks also appear to coincide with sea-level highstands and this may be the common link which accounts for increased organic carbon burial in different basins under different climatic and oceanic circulation regimes [14]. Increased volcanic activity may be the root cause of sea-level rise and/or climate change [e.g., 21]. It is notable that the Late Valanginian, Aptian and Cenomanian–Turonian $\delta^{13}C$ events correlate with major volcanic/rifting episodes, such as the Paraná volcanism in Brazil at 132 Ma [48] and onset of South Atlantic oceanic rifting during CM11 [49], the Ontong–Java volcanism at 123 Ma [44], and the extensive Madagascar basalts which are not precisely dated but are partially intercalated with Turonian sediments [50].

Acknowledgements

We are very grateful to H. Weissert, R. Bersezio, G. Muttoni, G. Mataloni, D. Valenti and A. Rottigni for help in the field. We acknowledge permission to work in the Pusiano quarry from Ing. Rey, and in the Breggia quarry from the *Dipartimento dell'Ambiente Ticino*. We have benefited from discussions with D. Hodell, R. Larson, H. Weissert, G. Muttoni and R. Bersezio, and from reviews by J. Ogg and two anonymous reviewers. R. Van der Voo supervised the review process. This research was supported by US National Science Foundation grant OCE-8915697, ETH project 0.20.305.89 and a MURST 40% grant to I. Premoli-Silva.

References

1 W.B. Harland, R.L. Armstrong, A.V. Cox, L.E. Craig, A.G. Smith and D.G. Smith, A Geologic Timescale, 1989, Cambridge University Press, Cambridge, 1990.
2 T.J. Bralower, Valanginian to Aptian calcareous nannofossil stratigraphy and correlation with the M-sequence magnetic anomalies, Mar. Micropaleontol. 11, 293–310, 1987.
3 J.E.T. Channell, T.J. Bralower and P. Grandesso, Biostratigraphic correlation of Mesozoic polarity chrons CM1 to CM23 at Capriolo and Xausa (Southern Alps, Italy), Earth Planet. Sci. Lett. 85, 203–221, 1987.

4 T.J. Bralower, S. Monechi and H.R. Thierstein, Calcareous nannofossil zonation of the Jurassic–Cretaceous boundary interval and correlation with the geomagnetic polarity timescale, Mar. Micropaleontol. 14, 143–235, 1989.
5 J.E.T. Channell and E. Erba, Early Cretaceous polarity chrons CM0 to CM11 recorded in northern Italian land sections near Brescia, Earth. Planet. Sci. Lett. 108, 161–179, 1992.
6 J.G. Ogg, Early Cretaceous magnetic polarity timescale and the magnetostratigraphy of Deep Sea Drilling Project Sites 603 and 534, western Central Atlantic, Init. Rep. DSDP 93, 849–880, 1987.
7 J.A. Tarduno, W.V. Sliter, T.J. Bralower, M. McWilliams, I. Premoli Silva and J.G. Ogg, M-sequence reversals recorded in DSDP sediment cores from the western Mid-Pacific Mountains and Magellan Rise, Geol. Soc. Am. Bull. 101, 1306–1316, 1989.
8 H. Weissert and A. Lini, Ice age interludes during the time of Cretaceous greenhouse climate? in: Controversies in Modern Geology, D.W. Müller, J.A. McKenzie and H. Weissert, eds., pp. 173–191, Academic Press, London, 1991.
9 A. Lini, H. Weissert and E. Erba, The Valanginian carbon isotope event: a first episode of greenhouse climate conditions during the Cretaceous, Terra Nova 4, 374–384, 1992.
10 P. Cotillon and M. Rio, Cyclic sedimentation in the Cretaceous of DSDP site 535 and 540 (Gulf of Mexico), 534 (central Atlantic) and the Vocontian Basin (France), Init. Rep. DSDP 77, 339–376, 1984.
11 H. Weissert, C-isotope stratigraphy, a monitor of paleoenvironmental change: a case study from the Early Cretaceous, Surv. Geophys. 10, 1–61, 1989.
12 P.A. Scholle and M.A. Arthur, Carbon isotope fluctuations in Cretaceous pelagic limestones: potential stratigraphic and petroleum exploration tool, Am. Assoc. Pet. Geol. Bull. 64, 67–87, 1980.
13 S.O. Schlanger, M.A. Arthur, H.C. Jenkyns and P.A. Scholle, The Cenomanian–Turonian oceanic anoxic event, I. Stratigraphy and distribution of organic carbon-rich beds and the marine $\delta^{13}C$ excursion, in: Marine Petroleum Source Rocks, J. Brooks and A.J. Fleet, eds., Geol. Soc. London Spec. Publ. 26, 371–399, 1987.
14 M.A. Arthur, S.O. Schlanger and H.C. Jenkyns, The Cenomanian–Turonian oceanic anoxic event, II. Paleoceanographic controls on organic matter production and preservation, in: Marine Petroleum Source Rocks. J. Brooks and A.J. Fleet, eds., Geol. Soc. London Spec. Publ. 26, 401–420, 1987.
15 M.A. Arthur, W.E. Dean and L.M. Pratt, Geochemical and climatic effects of increased marine organic carbon burial at the Cenomanian/Turonian boundary, Nature 335, 714–717, 1988.
16 H. Weissert, J.A. McKenzie and J.E.T. Channell, Natural variations in the carbon cycle during the Early Cretaceous, in: The Carbon Cycle and Atmospheric CO_2: Natural Variations Archean to Present, E.T. Sundquist and W.S. Broecker, eds., AGU Geophys. Monogr. 32, 531–545, 1985.
17 M.A. Arthur, W.E. Dean and S.O. Schlanger, Variations in the global carbon cycle during the Cretaceous related to climate, volcanism, and changes in atmospheric CO_2, in: The Carbon Cycle and Atmospheric CO_2: Natural Variations Archean to Present, E.T. Sundquist and W.S. Broecker, eds., AGU Geophys. Monogr. 32, 504–529, 1985.
18 W.H. Berger and E. Vincent, Deep sea carbonates: Reading the carbon-isotope signal, Geol. Rundsch. 75, 249–269, 1986.
19 E. Vincent and W.H. Berger, Carbon dioxide and polar cooling in the Miocene: The Monterey Hypothesis, in: The Carbon Cycle and Atmospheric CO_2: Natural Variations Archean to Present, E.T. Sundquist and W. Broecker, eds., AGU Geophys. Monogr. 32, 455–468, 1985.
20 K.B. Föllmi, H. Weissert and A. Lini, Nonlinearities in phosphogenesis and phosphorus–carbon coupling and their implications for global change, in: Interactions of C, N, P and S Biogeochemical Cycles and Global Change (NATO ASI Ser.), R. Wollast, F. Mackenzie et al., eds., pp. 447–474, Springer, Berlin, 1993.
21 R.L. Larson, Geological consequences of superplumes, Geology 19, 963–966, 1991.
22 T.D. Herbert, R.F. Stallard and A.G. Fischer, Anoxic events, productivity rhythms and the orbital signature in a mid-Cretaceous deep-sea sequence from central Italy, Paleoceanography 1, 495–506, 1986.
23 L.M. Pratt and J.D. King, Variable marine productivity and high eolian input recorded by rhythmic black shales in mid-Cretaceous pelagic deposits from central Italy, Paleoceanography 1, 507–522, 1986.
24 T.J. Bralower and H.R. Thierstein, Organic carbon and metal accumulation rates in Holocene and mid-Cretaceous sediments: palaeoceanographic significance, in: Marine Petroleum Source Rocks, J. Brooks and A.J. Fleet, eds., Geol. Soc. London Spec. Publ. 26, 345–369, 1987.
25 S.O. Schlanger and H.C. Jenkyns, Cretaceous anoxic events: causes and consequences, Geol. Mijnbouw 55, 179–184, 1976.
26 E.L. Winterer and A. Bosellini, Subsidence and sedimentation on a Jurassic passive continental margin, Southern Alps, Italy, Bull. Am. Assoc. Pet. Geol. 65, 394–421, 1981.
27 H. Weissert, Depositional processes in an ancient pelagic environment: the Lower Cretaceous Maiolica of the Southern Alps, Eclogae Geol. Helv. 74, 339–352, 1981.
28 M.A. Arthur and I. Premoli Silva, Development of widespread organic carbon-rich strata in the Mediterranean Tethys, in: Nature and Origin of Cretaceous Carbon-rich Facies, S.O. Schlanger and M.B. Cita, eds., pp. 7–54, Academic Press, London, 1982.
29 E. Erba and B. Quadrio, Biostratigrafia a nannofossili calcarei, Calpionellidi e Foraminiferi planctonici della Maiolica (Titoniano superiore-Aptiano) nelle Prealpi Bresciane (Italia settentrionale), Riv. Ital. Paleontol. Stratigr. 93, 3–108, 1987.
30 J.E.T. Channell, W. Lowrie and F. Medizza, Middle and Early Cretaceous magnetic stratigraphy from the Cismon section, Northern Italy, Earth Planet. Sci. Lett. 42, 153–166, 1979.
31 J.E.T. Channell and P. Grandesso, A revised correlation of Mesozoic polarity chrons to Calpionellid zones, Earth Planet. Sci. Lett. 85, 222–240, 1987.

32 J.A. Tarduno, Magnetic susceptibility cyclicity and magnetic dissolution in Cretaceous limestones of the Southern Alps (Italy), Geophys. Res. Lett. 19, 1515–1518, 1992.
33 J. VandenBerg and A.A.H. Wonders, Paleomagnetism of late Mesozoic pelagic limestones from the Southern Alps, J. Geophys. Res. 85, 3623–3627, 1980.
34 J.L. Kirschvink, The least squares line and plane and the analysis of paleomagnetic data, Geophys. J.R. Astron. Soc. 62, 699–718, 1980.
35 R.A. Fisher, Dispersion on a sphere. Proc. R. Soc. London, Ser. A 217, 295–305, 1953.
36 J.E.T. Channell, C. Doglioni and J.S. Stoner, Jurassic and Cretaceous paleomagnetic data from the Southern Alps (Italy), Tectonics 11, 811–822, 1992.
37 H.R. Thierstein, Lower Cretaceous calcareous nannoplankton biostratigraphy, Abh. Geol. Bundesanst. A 29, 1–52, 1973.
38 H.R. Thierstein, Mesozoic calcareous nannoplankton biostratigraphy of marine sediments, Mar. Micropaleontol. 1, 325–362, 1976.
39 Y. Aita and H. Okada, Radiolarians and calcareous nannofossils from the uppermost Jurassic and Lower Cretaceous strata of Japan and Tethyan regions, Micropaleontology 32, 97–128, 1986.
40 S. Monechi and H.R. Thierstein, Late Cretaceous–Eocene nannofossil and magnetostratigraphic correlations near Gubbio, Italy, Mar. Micropaleontol. 9, 419–440, 1985.
41 J.G. Ogg, R.W. Hasenyager, W.A. Wimbledon, J.E.T. Channell and T.J. Bralower, Magnetostratigraphy of the Jurassic–Cretaceous boundary interval—Tethyan and English faunal realms, Cretaceous Res. 12, 455–482, 1991.
42 F. Cecca, G. Palini, E. Erba, I. Premoli-Silva and R. Coccioni, Hauterivian–Barremian chronostratigraphy based on ammonites, nannofossils, planktonic foraminifera, and magnetic chrons from the Mediterranean domain, Cretaceous Res., submitted.
43 D.V. Kent and F.M. Gradstein, A Cretaceous and Jurassic geochronology, Geol. Soc. Am. Bull. 96, 1419–1427, 1985.
44 J.A. Tarduno, W.V. Sliter, L. Kroenke, M. Leckie, H. Mayer, J.J. Mahoney, R. Musgrave, M. Storey and E.L. Winterer, Rapid formation of the Ontong Java Plateau by Aptian mantle plume volcanism, Science 254, 399–403, 1991.
44a J.J. Mahoney, M. Storey, R. Duncan, K.J. Spencer and M. Pringle, Geochemistry and age of the Ontong–Java Plateau, in: Monograph on the Mesozoic Pacific (Schlanger Volume), M. Pringle, W. Sager and W. Sliter, eds., AGU, Washington, D.C., in press.
45 R.A. Berner, Sulfate reduction, organic matter decomposition and pyrite formation, Philos. Trans. R. Soc. London, Ser. A 315, 25–28, 1985.
46 D.E. Canfield and R.A. Berner, Dissolution and pyritization of magnetite in anoxic marine sediments, Geochim. Cosmochim. Acta 51, 645–659, 1987.
47 B.U. Haq, J. Hardenbol and P.R. Vail, Chronology of fluctuating sea levels since the Triassic, Science 235, 1156–1167, 1987.
48 P.R. Renne, M. Ernesto, I.G. Pacca, A.J.R. Nady, R.S. Coe, J.M. Glen, M. Prevot and M. Perrin, Age and duration of Paraná flood volcanism in Brazil, Eos 73 (43), 531–532, 1992.
49 P.D. Rabinowitz and J. LaBrecque, The Mesozoic South Atlantic Ocean and evolution of its continental margins, J. Geophys. Res. 84, 5973–6002, 1979.
50 J. Mahoney, C. Nicollet and C. Dupuy, Madagascar basalts: tracking oceanic and continental sources, Earth Planet Sci. Lett. 104, 350–363, 1991.